Quantum-Yield-Optimized Fluorophores for Site-Specific Labeling and Super-Resolution Imaging

Christian Grunwald,[†,ll] Katrin Schulze,[†,ll] Gregory Giannone,[‡,#] Laurent Cognet,[§] Brahim Lounis,[§] Daniel Choquet,[‡,#] and Robert Tampé*,[†]

[†]Institute of Biochemistry, Goethe-University Frankfurt, Max-von-Laue-Str. 9, D-60438 Frankfurt/M., Germany

[‡]University of Bordeaux, Interdisciplinary Institute for Neuroscience

[#]CNRS UMR 5297, F-33000 Bordeaux, France

[§]Laboratoire Photonique Numérique et Nanosciences, Université de Bordeaux, Institut d'Optique Graduate School and CNRS, 33405 Talence, France

S *Supporting Information*

ABSTRACT: Single-molecule applications, saturated pattern excitation microscopy, and stimulated emission depletion (STED) microscopy demand bright as well as highly stable fluorescent dyes. Here we describe the synthesis of quantum-yield-optimized fluorophores for reversible, site-specific labeling of proteins or macromolecular complexes. We used polyproline-II (PPII) helices as sufficiently rigid spacers with various lengths to improve the fluorescence signals of a set of different *tris*NTA—fluorophores. The improved quantum yields were demonstrated by steady-state and fluorescence lifetime analyses. As a proof of principle, we characterized the *tris*NTA—PPII—fluorophores with respect to in vivo protein labeling and super-resolution imaging at synapses of living neurons. The distribution of His-tagged AMPA receptors (GluA1) in spatially restricted synaptic clefts was imaged by confocal and STED microscopy. The comparison of fluorescence intensity profiles revealed the superior resolution of STED microscopy. These results highlight the advantages of biocompatible and, in particular, small and photostable *tris*NTA—PPII—fluorophores in super-resolution microscopy.

Single-molecule applications, saturated pattern excitation microscopy, and stimulated emission depletion (STED) microscopy demand bright and highly stable fluorescent dyes.[1,2] Despite intensive research, the choice of fluorophores is still very limited. Typically, a stable fluorescent dye is covalently attached to the target. This methodology brings forward a number of limitations, particularly in the case of protein labeling. First of all, the fluorescent probes need to be attached selectively and site-specifically to prevent unspecific background. This often requires single cysteine mutations in a cysteine-less background for covalent protein modification. Employing quantum dots allows photobleaching problems to be overcome.[3–6] In spite of recent progress in the synthesis of quantum dots with hydrodynamic diameters close to 10 nm,[7,8] their downside is still their large size, rendering the probes inaccessible to spatially confined architectures. In addition, issues regarding biocompatibility, stability, and multivalency due to proper particle coating and functionalization must be taken into account.[6,9,10] Here we propose a new method for tackling the problems outlined above.

The reversible NTA—histidine interaction has been widely used, but its applicability for site-specific labeling and single-molecule techniques has been severely hampered because of the very transient interaction (k_{off} = 1 s^{-1}, K_d = 14 μM).[11,12] We therefore developed the multivalent chelator heads *bis*-, *tris*-, and *tetrakis*NTA, which can boost the NTA—histidine affinity to the subnanomolar range (K_d = 0.1 nM).[12,13] These multivalent NTA chelator heads are modular and allow for site-specific labeling and two-dimensional organization of proteins via self-assembly.[14–19]

Photostable fluorophores with high quantum yields are demanded by single-molecule superlocalization methods.[1,2,20] However, if the above-mentioned metal-loaded chelator heads and excited fluorophores are in close proximity, the emission is quenched by conversion into heat.[16] To maximize the quantum yield, we chose to use polyproline-II (PPII) helices as sufficiently rigid spacers with various lengths (these are denoted as P$_x$, where x is the number of prolyl residues).[21–24] Thereby, the fluorophores and metal ions could be separated by well-defined distances. Figure 1 presents quantum-yield-optimized *tris*NTA—P$_n$—fluorophores with n = 0, 4, 8, and 12.

Drastically increased fluorescence signals were observed with *tris*NTA—PPII—fluorophores, which were strongly correlated with the length of the PPII helix. In contrast, flexible oligo-(ethylene glycol) (OEG) spacers did not prevent the strong fluorescence quenching.[16] In addition to variation of the spacer length, different fluorophores, such as Oregon Green 488 (OG488) and ATTO565, were attached to the *tris*NTA—PPPII units. Notably, ATTO565 is more sensitive to quenching than OG488. Quenching phenomena are generally described by the Stern—Volmer equation, taking into account dynamic (e.g., by molecular collision) and static (e.g., by complex formation) mechanisms.[25]

In our system, the steady-state quantum yield was reduced via static and dynamic quenching processes, most likely based on photoinduced electron transfer (PET). Noticeably, OG488 and ATTO565 showed different quenching for the same spacer length. For all of the fluorophores examined, the steady-state
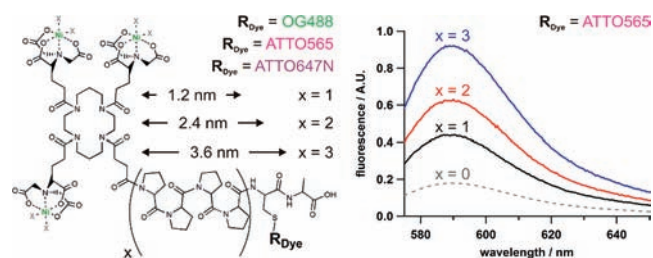
Figure 1. (left) Flexible modular concept of a *tris*NTA chelator head separated from a fluorescent probe (OG488, ATTO565, or ATTO647N) by rigid PPII helices of different lengths. (right) Normalized fluorescence spectra demonstrating the fluorescence quenching as a function of separation distance. A fluorescence intensity of 1.0 represents an unquenched fluorophore. Results are shown for *tris*NTA−P_n−ATTO565 in solution ($n = 0, 4, 8,$ and 12).
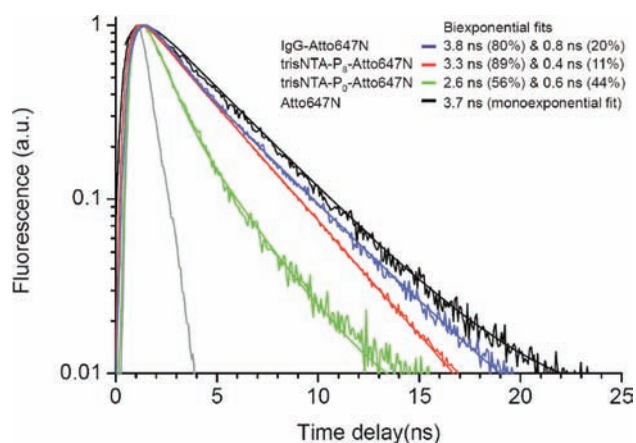
Figure 2. Fluorescence decays of different ATTO647N species recorded using a conventional time-correlated single-photon counting (TCSPC) setup. Excitation was performed by means of an optical parametric oscillator (~4 ps pulses) pumped by a Ti:Sa oscillator. A pulse picker was used to reduce the repetition rate of the laser system to 8 MHz. Fluorescence decays were fitted to biexponential functions (except for ATTO647N, which was satisfactorily fitted to a monoexponential curve). *Tris*NTA−P_0−ATTO647N (green) showed the fastest fluorescence decay. In contrast, the polyproline spacer in *tris*NTA−P_8−ATTO647N (red) exhibited a fluorescence lifetime comparable to those of free (black) and IgG-bound (blue) ATTO647N. The instrumental response function is plotted in gray. As a result of quenching, the decay rate of *tris*NTA−P_0−ATTO647N (without a spacer) was increased by 40% relative to ATTO647N.

quantum yield was inversely correlated with the minimal linker distance.[26] Complementarily, fluorescence decay measurements were performed for different ATTO647N fluorophores, demonstrating that the P_8 spacer established fluorescence decays comparable to free and IgG-bound ATTO647N (Figure 2). Omitting the prolyl spacer increased the fluorescence decay rate by >40%, which is in agreement with previous findings.[27] In summary, the novel *tris*NTA−P_x−fluorophores resulted in a 5-fold higher quantum yield (Table 1).

We next characterized the *tris*NTA−PPII−fluorophores regarding in vivo protein labeling and super-resolution imaging within the synaptic cleft of living neurons. We incubated rat hippocampal neuron for 10 min with *tris*NTA−P_8−ATTO647N to study the distribution of His-tagged AMPA receptor complexes

Table 1. Fluorescence Quenching of *Tris*NTA−P_n−Fluorophores as a Function of the Distance between the Ni^{2+}-Loaded Chelator Head and the Fluorophore for Two Different Fluorescent Dyes (OG488 and ATTO565)[a]

compound	no. of prolines	NTA−fluorophore distance (nm)	quenching (%)
*tris*NTA−P_0− OG488 (**1**)	0	0	53
*tris*NTA−P_0− ATTO565 (**2**)			82
*tris*NTA−P_4− C(OG488)A (**6**)	4	1.2	45
*tris*NTA−P_4− C(ATTO565)A (**7**)			48
*tris*NTA−P_8− C(OG488)A (**8**)	8	2.4	25
*tris*NTA−P_8− C(ATTO565)A (**9**)			18
*tris*NTA−P_{12}− C(OG488)A (**10**)	12	3.6	13
*tris*NTA−P_{12}− C(ATTO565)A (**11**)			9

[a] Two dyes were used in order to characterize the influence of the fluorescent probe on the quenching phenomenon.
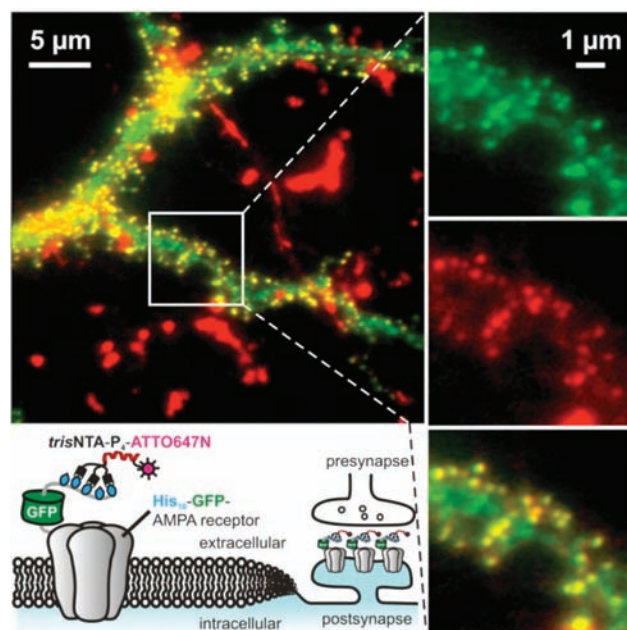
Figure 3. Live staining of a rat hippocampal neuron (20 days after division) transfected with His_{10}-tagged GFP−GluA1 AMPA receptor subunit using *tris*NTA−P_8−ATTO647N (10 min at room temperature). (bottom left) Schematic of the experiment. (top left) Overlay of wide-field dual-color fluorescence images. Localization of GluA1 in dendritic spines is revealed by the GFP signal (green; ex/em 485 ± 20/525 ± 40 nm), while colocalization with *tris*NTA−P_8−ATTO647N (red; ex/em 565 ± 30/655 ± 20 nm) appears in yellow. (right) Magnified insets that show the separated fluorescence channels, demonstrating the accessibility of *tris*NTA−P_8−ATTO647N to the synaptic GluA1.
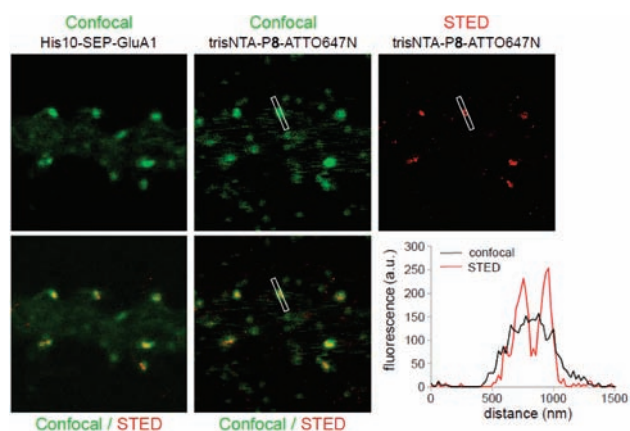
Figure 4. Confocal (green) and super-resolution STED (red) fluorescence images (ex/em 635/655 nm; depletion 750 nm) of the $trisN$-TA$-P_8-$ATTO647N signal displaying the localization of GluA1 in dendritic spines from the same section. Intensity profiles of a region of interest (white frame) are given in the illustration at the lower-right. The experimental conditions are identical to those in Figure 3. Resolution of 100 nm synaptic clusters of GluA1 was achieved.

(GluA1) by confocal microscopy (Figure 3). The colocalization of green fluorescent protein (GFP) (green channel) and the $tris$NTA$-P_8-$fluorophore (red) illustrates the specific labeling of His10-tagged GFP$-$GluA1 receptors in live cells. The direct comparison by confocal and STED microscopy reveals the superior resolution of STED microscopy (Figure 4). These results highlight the advantages of biocompatible and, in particular, small and photostable fluorophores in super-resolution microscopy.

In conclusion, the most appealing features of our quantum-yield-optimized $tris$NTA$-PPII-$fluorophores can be summarized as follows: Contrary to quantum dots, no toxic effects have been reported for $tris$NTA$-$fluorophores used in vivo (e.g., intracellular particle tracking).[28] A prevailing drawback of saturated pattern excitation microscopy is photobleaching of the employed fluorescent probes, for which the inherent reversibility of the NTA$-$histidine interaction can compensate, as fresh $tris$NTA$-P_x-$fluorophores from the bulk can replenish photobleached fluorophores once they are attached to their histidine-tagged targets. A further benefit of this approach is that imaging bandwidth is conserved even when dealing with rather fast molecular dynamics, whereas conventional image acquisition strategies significantly struggle to maintain good signal-to-noise levels.[29]

Using quantum-yield-optimized $tris$NTA$-PPII-$fluorophores, we were able to image and track single receptors in native cell membranes with high spatiotemporal resolution (<50 nm).[20] Finally, the newly developed high-quantum, site-specific $tris$N-TA$-PP2-$fluorophores can specifically visualize single cellular targets even in complex biological substructures (e.g., neuronal synapses), which are difficult to access with conventional fluorescent probes.

ASSOCIATED CONTENT

ⓢ **Supporting Information.** Detailed information regarding synthesis, spectroscopic characterization, specific protein binding, and in vivo visualization of $tris$NTA$-P_x-$fluorophores in living neurons; complete ref 18. This material is available free of charge via the Internet at http://pubs.acs.org.

AUTHOR INFORMATION

Corresponding Author
tampe@em.uni-frankfurt.de

Author Contributions
[||]These authors contributed equally.

REFERENCES

(1) Hell, S. W. *Science* **2007**, *316*, 1153.
(2) Fernandez-Suarez, M.; Ting, A. Y. *Nat. Rev. Mol. Cell. Biol.* **2008**, *9*, 929.
(3) Chan, W. C. W.; Maxwell, D. J.; Gao, X. H.; Bailey, R. E.; Han, M. Y.; Nie, S. M. *Curr. Opin. Biotechnol.* **2002**, *13*, 40.
(4) Chan, W. C. W.; Nie, S. M. *Science* **1998**, *281*, 2016.
(5) Heine, M.; Groc, L.; Frischknecht, R.; Beique, J. C.; Lounis, B.; Rumbaugh, G.; Huganir, R. L.; Cognet, L.; Choquet, D. *Science* **2008**, *320*, 201.
(6) Gao, X. H.; Yang, L. L.; Petros, J. A.; Marshal, F. F.; Simons, J. W.; Nie, S. M. *Curr. Opin. Biotechnol.* **2005**, *16*, 63.
(7) Howarth, M.; Liu, W.; Puthenveetil, S.; Zheng, Y.; Marshall, L. F.; Schmidt, M. M.; Wittrup, K. D.; Bawendi, M. G.; Ting, A. Y. *Nat. Methods* **2008**, *5*, 397.
(8) Liu, W.; Greytak, A. B.; Lee, J.; Wong, C. R.; Park, J.; Marshall, L. F.; Jiang, W.; Curtin, P. N.; Ting, A. Y.; Nocera, D. G.; Fukumura, D.; Jain, R. K.; Bawendi, M. G. *J. Am. Chem. Soc.* **2010**, *132*, 472.
(9) Kirchner, C.; Liedl, T.; Kudera, S.; Pellegrino, T.; Javier, A. M.; Gaub, H. E.; Stolzle, S.; Fertig, N.; Parak, W. J. *Nano Lett.* **2005**, *5*, 331.
(10) Derfus, A. M.; Chan, W. C. W.; Bhatia, S. N. *Nano Lett.* **2004**, *4*, 11.
(11) Dorn, I. T.; Neumaier, K. R.; Tampé, R. *J. Am. Chem. Soc.* **1998**, *120*, 2753.
(12) Lata, S.; Reichel, A.; Brock, R.; Tampé, R.; Piehler, J. *J. Am. Chem. Soc.* **2005**, *127*, 10205.
(13) Tinazli, A.; Tang, J. L.; Valiokas, R.; Picuric, S.; Lata, S.; Piehler, J.; Liedberg, B.; Tampé, R. *Chem.—Eur. J.* **2005**, *11*, 5249.
(14) Lata, S.; Piehler, J. *Nat. Protoc.* **2006**, *1*, 2104.
(15) Lata, S.; Gavutis, M.; Piehler, J. *J. Am. Chem. Soc.* **2006**, *128*, 6.
(16) Lata, S.; Gavutis, M.; Tampé, R.; Piehler, J. *J. Am. Chem. Soc.* **2006**, *128*, 2365.
(17) Lata, S.; Piehler, J. *Anal. Chem.* **2005**, *77*, 1096.
(18) Artelsmair, H.; *Small* **2008**, *4*, 847.
(19) Tinazli, A.; Piehler, J.; Beuttler, M.; Guckenberger, R.; Tampé, R. *Nat. Nanotechnol.* **2007**, *2*, 220.
(20) Giannone, G.; Hosy, E.; Levet, F.; Constals, A.; Schulze, K.; Sobolevsky, A. I.; Rosconi, M. P.; Gouaux, E.; Tampé, R.; Choquet, D.; Cognet, L. *Biophys. J.* **2010**, *99*, 1303.
(21) Cowan, P. M.; McGavin, S. *Nature* **1955**, *176*, 501.
(22) Williamson, M. P. *Biochem. J.* **1994**, *297*, 249.
(23) Schuler, B.; Lipman, E. A.; Steinbach, P. J.; Kumke, M.; Eaton, W. A. *Proc. Natl. Acad. Sci. U.S.A.* **2005**, *102*, 2754.
(24) Stryer, L.; Haugland, R. P. *Proc. Natl. Acad. Sci. U.S.A.* **1967**, *58*, 719.

(25) Moon, A. Y.; Poland, D. C.; Scheraga, H. A. *J. Phys. Chem.* **1965**, *69*, 2960.

(26) We note that the molar mass of the different *tris*NTA—P_x—fluorophores varies within roughly 30%, which hardly affects the diffusion coefficient. Therefore, the different molecules can be considered to be the same size and travel at the same speed. Thus, the frequency of collisions is almost constant.

(27) Doose, S.; Neuweiler, H.; Barsch, H.; Sauer, M. *Proc. Natl. Acad. Sci. U.S.A.* **2007**, *104*, 17400.

(28) Orange, C.; Specht, A.; Puliti, D.; Sakr, E.; Furuta, T.; Winsor, B.; Goeldner, M. *Chem. Commun.* **2008**, 1217.

(29) Fujiwara, T.; Ritchie, K.; Murakoshi, H.; Jacobson, K.; Kusumi, A. *J. Cell Biol.* **2002**, *157*, 1071.

8093

dx.doi.org/10.1021/ja200967z |*J. Am. Chem. Soc.* 2011, 133, 8090–8093